Highlights

Privacy-Preserving Multi-VPPs Scheduling for Peak Ramp Minimization

Weile Kong, Hongxing Ye, Yinyin Ge, Wangqing Mao, Song Gao

- Virtual power plants meet ramping demand with local distributed resources dispatch.
- The proposed location-aware VPP model can reduce power losses.
- The location-aware VPP schedule improves the voltage performance of the PDN.
- The proposed ADMM-like framework enables VPPs and PDN to conduct local optimization.

Privacy-Preserving Multi-VPPs Scheduling for Peak Ramp Minimization

Weile Kong[a], Hongxing Ye[a,*], Yinyin Ge[a], Wangqing Mao[a], Song Gao[b]

[a]*School of Automation Science and Engineering, Xi'an Jiaotong University, 710049, Xi'an, China*
[b]*State Grid Shandong Electric Power Research Institute, 250003, Jinan, China*

Abstract

The increasing integration of distributed energy resources (DERs) has driven the transformation of active distribution systems. A large volume of small-capacity DERs results in various distribution system operational challenges, such as ramping events, overvoltage issues, privacy concerns, etc. The virtual power plant (VPP) emerges as a promising solution. Effective coordination between power distribution networks and multi-VPPs (MVPPs) is imperative for mitigating peak ramp. This paper introduces a novel peak ramp minimization model for MVPP systems in active distribution networks. The proposed model incorporates location-aware MVPP power exchanges, reducing distribution losses and operational costs. By integrating the Karush-Kuhn-Tucker condition into the Alternating Direction Method of Multipliers (ADMM), we propose a novel ADMM-like algorithm for decentralized energy management. The ADMM-like algorithm enables local optimization for each VPP and preserves privacy. Numerical simulations demonstrate that the proposed approach effectively minimizes the peak ramp, reduces power losses, and mitigates computational and communication burdens.

Keywords: Peak ramp minimization, privacy preservation, multi-virtual power plants, ADMM-like algorithm

1. Introduction

1.1. Motivations

Motivated by the energy transition trend and global environmental policies in recent years, distributed energy resources (DERs) such as photovoltaic (PV) power, micro gas turbine (MGT), and battery energy storage (BES) have experienced rapid development [1]. According to the IEA's report, 167 GW of distributed PV capacity was added globally from 2019 to 2021, and the global electric vehicle (EV) stock exceeded 10 million in 2020 [2]. This trend has resulted in a transition from traditional to active distribution systems characterized by multiple independent small-scale DERs [3]. The proliferation of these distributed resources, characterized by their large quantity, small scale, and widespread distribution, introduces new challenges to the operation of power distribution networks (PDNs). High penetration of distributed energy resources may cause extreme ramp events, substantial computation burdens, and privacy concerns.

It has been demonstrated that a virtual power plant (VPP) can effectively aggregate large-scale small-capacity prosumers, offering a viable solution for efficient DER management [4]. The management and dispatch strategies of VPPs have received much attention in the power community. In [5], an optimal energy and reserve scheduling scheme for VPPs is proposed with demand-side flexible resources. It utilizes model predictive control and receding-horizon optimization to develop an adaptive and predictive strategy for the real-time optimal power dispatch of VPPs. Additionally, in [6], a tri-layer coordinated operation framework for the VPP with multiple DER aggregators is introduced. The authors transform the framework into a Mixed Integer Linear Programming (MILP) problem by leveraging Karush-Kuhn-Tucker (KKT) optimal conditions and the strong duality theorem. In [7], a pricing-based bilevel model is proposed for collaborative energy management in an active distribution network with multi-VPPs (MVPPs), aiming to enhance system security and economic performance. Similarly, a bilevel model is introduced in [8] for collaborative operation in the active distribution system with MVPPs, facilitating DERs' participation in the energy and reserve market. These models are optimized using a centralized method that transforms the bilevel framework into a single-level problem based on KKT conditions. Despite the advancements in these studies, it is worth noting that most of them overlook concerns related to privacy and computation burden within the centralized control scheme.

1.2. Literature Review and Current Gaps

Distributed optimization methods offer significant advantages over centralized approaches, particularly in scalability, information privacy, decision independence, and reduced computational and communication burdens. These methods can generally be categorized into two main classes based on their decomposition characteristics: Lagrangian relaxation-based methods and primal decomposition (PD) methods. Below, we outline each approach and discuss key techniques within these categories.

1) Lagrangian Relaxation-Based Methods: One prominent method in this category is the dual decomposition method,

*Corresponding author
Email address: yehxing@xjtu.edu.cn (Hongxing Ye)

which leverages the separable structure of the Lagrangian function to enable distributed optimization. However, dual decomposition can encounter convergence issues in certain scenarios. To address these limitations, the Alternating Direction Method of Multipliers (ADMM) was introduced, incorporating an augmented Lagrangian term to improve convergence performance [9]. While ADMM is effective, it requires a central coordinator and cannot guarantee convergence when applied to nonconvex problems. In addition to dual decomposition and ADMM, other distributed techniques based on KKT conditions have been proposed to enhance separability. For instance, Optimality Condition Decomposition (OCD) divides the original problem into smaller subproblems by solving the KKT conditions [10]. However, OCD requires the Lipschitz-continuous second-order derivatives of the problem, which can limit its applicability. Another technique, the Dual Projection Subgradient (DPS) method, is designed for mixed-integer linear programming (MILP) problems, excelling in cases with pure binary programming subproblems [11]. Nevertheless, DPS may encounter convergence challenges due to the absence of penalty terms in its formulation.

2) Primal Decomposition-Based Methods: The second class of distributed methods focuses on primal decomposition, including techniques such as generalized Benders decomposition (BD) and multi-parametric quadratic programming. BD is a widely used approach that splits the problem into a master problem and subproblems [12]. While effective, BD requires adding new variables and constraints to the model, which can lead to significant computational overhead. More recently, distributed algorithms based on parametric programming have gained attention. For example, the method proposed in [13] introduces an approach to handle distributed optimization via parametric techniques. However, these algorithms face challenges in managing high-dimensional parameters, which can impact their scalability and efficiency.

Various distributed operation strategies have been introduced in power systems with computational efficiency and decision independence in mind. A fully decentralized VPP energy-sharing model aimed at maximizing social welfare is formulated in [14], tackled through a partial-update ADMM approach. A primal-dual-based distributed method with dynamic weights is introduced in [15] to dispatch the power resources in each microgrid locally. It has a lower communication burden and lower computational complexity. However, they omit the network constraints and power losses. Similarly, a distributed accelerated dual descent algorithm is proposed in [16] to regulate nodal voltage by optimizing DERs' reactive power in distribution networks, which uses a lossless linearized DistFlow model. Considering power losses, authors in [17] develop a distributed fixed-time consensus method to realize the economic dispatch and demand response based on cooperative resource management within microgrids. A two-stage robust energy management strategy is established in a fully distributed manner for networked microgrids cost minimization [18]. The column-and-constraint generation algorithm embedded in ADMM is proposed to address the energy management problem using a relaxed DistFlow model, a power flow model designed for radial distribution networks. The nested framework requires frequent information exchange. While these studies effectively tackle computational complexities and consider power losses, it is noteworthy that information exchange analysis is often overlooked.

Various strategies have been proposed to address the ramping issue. For instance, a storage-based ramp rate control architecture is proposed in [19] to smooth and shift the net load for the high amount of PV penetration systems. The netload smoothing is realized based on a centralized least square minimization problem. It is modeled in a centralized manner. An OCD-based security-constrained demand response model is developed in [20] to balance the demand-supply chain and reduce the peak-to-valley ratio, which can reduce the ramping burden. An ADMM-based incentive mechanism is designed in [21] to minimize peak ramp with microgrids, which doesn't consider the network model. Nevertheless, the distributed peak ramp minimization, especially with location-aware lossy VPP operation, has received limited attention. It is noteworthy that unlike the most relevant research [22], which realizes ramp control by adding a rigid maximum ramping limit, the peak ramp consistently remains below an optimized variable value in this work. Table 1 provides a comparison between this work and the existing literature on ramping management.

Table 1: Comparison with Select Representative Works in the Literature.

# Ref.	Centralized	Distributed	Power Losses Modeling	Network Modeling	Ramping Management
[19]	✓				ramping constraints
[20]		✓		✓	peak-to-valley ratio minimization
[21]		✓			optimize peak ramp
[22]		✓	✓	✓	ramping constraints
This paper		✓	✓	✓	optimize peak ramp

1.3. Contributions

To bridge the identified research gaps, this study introduces a generalized model to minimize peak ramps in collaboration between the DSO and MVPPs, considering power losses. With computational burdens and privacy concerns in mind, we propose an innovative distributed ADMM-like algorithm based on Lagrangian relaxation and KKT conditions. The major contributions are summarized below.

- A novel peak ramp minimization model is formulated that incorporates privacy preservation, computational burdens, and power losses for the operation of distribution system operator (DSO) with MVPPs. It differs from the existing literature, such as [19] that relies on the centralized model or [21] that omits the distribution network model and power losses.
- The location-aware proposed model for MVPPs is more practical for distribution networks, which can reduce power losses and improve the voltage performance of PDN. This facilitates precise power dispatch, profit maximization, and loss allocation.
- A novel ADMM-like algorithm is proposed to solve the peak ramp minimization problem. Using the KKT stationarity condition, the global coupling inequality constraints associated with the peak ramp are effectively addressed. Subsequently, the collaborative optimization problem is decomposed into a DSO and N VPP subproblems.

- The proposed ADMM-like algorithm offers notable advantages, including reduced communication requirements compared to ADMM [9], resolution of convergence issues seen in DPS [11], and less frequent information exchange compared to primal decomposition-based methods [12, 13].
- A fully decentralized framework based on an ADMM-like algorithm is developed to achieve a local power schedule within individual DSO or VPP agents. The proposed framework demonstrates the scalability and the ability to achieve the optimal (or near-optimal) solution for both the DSO and MVPPs.

The remainder of this paper is organized as follows. Section II introduces the proposed peak ramp minimization model considering power loss. The proposed distributed optimization framework is presented in section III. Case studies are conducted in section IV. Section V concludes the paper and discusses future work.

2. Problem Formulation

This section introduces a collaborative power scheduling model for the DSO and MVPPs. The implementation scene of the proposed scheme is built in the day-ahead market environment. Thus, price fluctuations and renewable energy uncertainties are not modeled in the optimization problem. In addition, the economic weight of a single power distribution system is not enough to affect the market clearing price [7]. The proposed methodology is still applicable when uncertainty is considered, such as in scenario-based or chance-constrained approaches.

As shown in Fig. 1, the power distribution system is connected to the main grid, and multiple VPPs are within the distribution network. The power purchasing price from the power market is the local marginal price (LMP). We assume that DSO and VPPs operate in a cooperative fashion. The objective function (1) is to minimize the total operation cost of DSO and MVPPs.

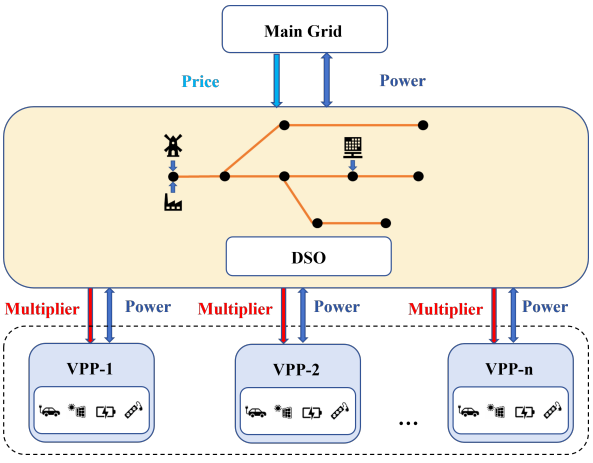

Figure 1: The interaction of the distribution system with MVPPs.

$$\min_{\boldsymbol{x},\boldsymbol{P}} f = f^{\text{dso}} + \sum_{k\in\mathcal{K}} f_k^{\text{vpp}} \tag{1}$$

where $\mathcal{K}$ is the set of VPPs. f^{dso} denotes the DSO's objective, which is formulated in (2).

$$f^{\text{dso}} = a_1\phi + a_2 \sum_{t\in\mathcal{T}} c_{0,t}P_{1,t} + a_2 \sum_{t\in\mathcal{T}}\sum_{i\in\mathcal{I}} P_{i,t} \tag{2}$$

$a_1\phi$ in eq. (2) is the peak ramp regulation term, which is similar to [21]. The second term, $a_2 \sum_{t\in\mathcal{T}} c_{0,t}P_{1,t}$, is the total electricity purchasing cost. The third term, $a_2 \sum_{t\in\mathcal{T}}\sum_{i\in\mathcal{I}} P_{i,t}$, is the power loss regulation term. In eq. (2), ϕ is the maximum ramp. $P_{i,t}$ is the bus injection power, and $P_{1,t}$ is the exchanged power between DSO and the main grid. a_1 and a_2 are the objective weights associated with peak ramp regulation and monetary electricity cost. $c_{0,t}$ is the LMP. $\mathcal{T}$ and $\mathcal{I}$ are sets of time and nodes, respectively.

In eq. (1), f_k^{vpp} denotes the kth VPP's objective, and it is formulated as below.

$$\begin{aligned} f_k^{\text{vpp}} = a_2 \sum_{t\in\mathcal{T}} \Big(c_1 \sum_{m\in\Omega_k^r} P_{m,t}^{\text{pv}} + c_2 \sum_{g\in\Omega_k^g} P_{g,t}^{\text{mgt}} + c_3 \sum_{b\in\Omega_k^b} P_{b,t}^{\text{e2h}} \Big) \\ + a_3 \sum_{t\in\mathcal{T}} \sum_{b\in\Omega_k^b} (H_{b,t} - H_{b,t}^{\text{ref}})^2 \end{aligned} \tag{3}$$

In the right-hand side of eq. (3), the first term is the operational cost of flexible resources such as photovoltaic (PV), micro gas turbine (MGT), and controllable thermal load (CTL). The second term denotes the user's discomfort associated with temperature regulation. In eq. (3), $P_{m,t}^{\text{pv}}$ is the output of PV unit. $P_{g,t}^{\text{mgt}}$ is the output of MGT. $a_3 = 1 - a_1 - a_2$ is the objective weight associated with the comfort deviation penalty. c_1, c_2, and c_3 are unit operation costs of PV, MGT, and CTL. Ω_k^* is the set of different DERs in the kth VPP. $H_{b,t}$ denotes the temperature in the building b at time t. $H_{b,t}^{\text{ref}}$ is the reference temperature in building b at time t. $P_{b,t}^{\text{e2h}}$ is the power consumed to serve thermal load.

2.1. DSO Operation Model

PDN can exchange power with the main grid and MVPPs to meet the load demand. To make a good tradeoff between computational efficiency and accuracy, we adopt an iterative linearized power flow model here [23]. Compared to the commonly used direct current optimal power flow (DC-OPF) model, the applied power flow model incorporates power losses and voltage magnitudes, which are critical in this context as the DSO and VPP entities aim to minimize losses while ensuring system security. The DSO operation model is detailed as follows.

$$-\phi \le r_t \le \phi, \forall t \in \mathcal{T} \tag{4}$$

$$r_t = \Big(\sum_{i\in\mathcal{I}} L_{i,t}^{\text{p}} - \sum_{k\in\mathcal{K}} P_{k,t}^{\text{fvpp}}\Big) - \Big(\sum_{i\in\mathcal{I}} L_{i,t-1}^{\text{p}} - \sum_{k\in\mathcal{K}} P_{k,t-1}^{\text{fvpp}}\Big) \tag{5}$$

$$P_{i,t} = \sum_{k\in\mathcal{I}^i} P_{k,t}^{\text{fvpp}} - L_{i,t}^{\text{p}}, \quad Q_{i,t} = \sum_{k\in\mathcal{I}^i} Q_{k,t}^{\text{fvpp}} - L_{i,t}^{\text{q}} \tag{6}$$

$$P_{i,t} = \sum_{(i,j)\in\mathcal{B}^i} P^{\text{line}}_{ij,t}, \quad Q_{i,t} = \sum_{(i,j)\in\mathcal{B}^i} Q^{\text{line}}_{ij,t} \tag{7}$$

$$P^{\text{line}}_{ij,t} = g_{ij}\left(\frac{v^2_{i,t}-v^2_{j,t}}{2}+\tilde{\theta}_{ij,t}\theta_{ij,t}-\frac{1}{2}\tilde{\theta}^2_{ij,t}\right)-b_{ij}\theta_{ij,t} + \left[g_{ij}\frac{\tilde{v}_{i,t}-\tilde{v}_{j,t}}{\tilde{v}_{i,t}+\tilde{v}_{j,t}}\left(v^2_{i,t}-v^2_{j,t}\right)+\frac{g_{ij}}{2}\left(\tilde{v}^2_{i,t}-\tilde{v}^2_{j,t}\right)^2\right] \tag{8}$$

$$Q^{\text{line}}_{ij,t} = b_{ij}\left(\frac{v^2_{j,t}-v^2_{i,t}}{2}-\tilde{\theta}_{ij,t}\theta_{ij,t}+\frac{1}{2}\tilde{\theta}^2_{ij,t}\right)-g_{ij}\theta_{ij,t} -\left[b_{ij}\frac{\tilde{v}_{i,t}-\tilde{v}_{j,t}}{\tilde{v}_{i,t}+\tilde{v}_{j,t}}\left(v^2_{i,t}-v^2_{j,t}\right)+\frac{b_{ij}}{2}\left(\tilde{v}^2_{i,t}-\tilde{v}^2_{j,t}\right)^2\right] \tag{9}$$

$$v^2_{i,\min} \le v^2_{i,t} \le v^2_{i,\max}, \quad \forall i \in \mathcal{I}, \forall t \in \mathcal{T} \tag{10}$$

Inequality constraint (4) defines the peak ramp demand. Equation (5) denotes the ramping demand. $L^{\text{p}}_{i,t}$ and $L^{\text{q}}_{i,t}$ represent the active and reactive load demands for node i at time t, respectively. $P^{\text{fvpp}}_{k,t}$ and $Q^{\text{fvpp}}_{k,t}$ are the DS's received real and reactive power from VPP, respectively. The nodal power injection is defined in (6). Constraint (7) represents the power balance equations. Equation (8) and (9) can be treated as linear power flow constraints by regarding $v^2_{i,t}$ as an independent variable. Besides, $\tilde{\theta}_{ij,t}$ and $\tilde{v}_{ij,t}$ are given parameters obtained from the last iteration. Voltage range is constrained in (10). $\mathcal{I}^i$ and $\mathcal{B}^i$ are sets of VPPs and branches linked to node i, respectively.

2.2. VPP Operation Model

In this section, we establish individual models for each VPP. VPP can include various DERs, such as PV, MGT, BES, and CTL. Let $P^{\text{tds}}_{k,t}$ denote the combined power output of VPP. It is formulated as follows.

$$P^{\text{tds}}_{k,t} = \sum_{m\in\Omega^r_k} P^{\text{pv}}_{m,t} + \sum_{g\in\Omega^g_k} P^{\text{mgt}}_{g,t} + \sum_{e\in\Omega^e_k} P^{\text{es}}_{e,t} - \sum_{b\in\Omega^b_k} P^{\text{e2h}}_{b,t} \tag{11}$$

$P^{\text{tds}}_{k,t}$ also represents the power exchange between VPP and DS. It is noteworthy that the power exchange can occur bidirectionally. The positive value means power flows from the VPP to the DS while a negative value indicates the opposite direction.

2.2.1. PV Constraint

Rooftop PV, characterized by its small-scale nature, can be aggregated by VPPs to participate in the electricity market. It should be limited by the forecasted output.

$$0 \le P^{\text{pv}}_{m,t} \le P^{\text{pvf}}_{m,t} \tag{12}$$

2.2.2. MGT Constraint

Given the rapid ramping capabilities of MGTs, we opt for a simplified MGT model in this context. The output range of the MGT is constrained between 0 and its maximum output power.

$$0 \le P^{\text{mgt}}_{g,t} \le P^{\text{mgt}}_{g,\max} \tag{13}$$

2.2.3. Storage Constraint

The storage output can be represented by its discharging ($P^{\text{d}}_{e,t}$) or charging power ($P^{\text{c}}_{e,t}$). Binary indicators $u^{\text{c}}_{e,t}$ and $u^{\text{d}}_{e,t}$ represent the charge/discharge status. Constraint (15) ensures the battery does not charge and discharge simultaneously. Power and capacity limits are constrained in (16) and (17). Time-coupled energy level ($E_{e,t}$) is formulated in (18).

$$P^{\text{es}}_{e,t} = P^{\text{d}}_{e,t} - P^{\text{c}}_{e,t} \tag{14}$$

$$0 \le u^{\text{c}}_{e,t} + u^{\text{d}}_{e,t} \le 1 \tag{15}$$

$$0 \le P^{\text{c}}_{e,t} \le u^{\text{c}}_{e,t} P^{\text{c}}_{e,max}, \quad 0 \le P^{\text{d}}_{e,t} \le u^{\text{d}}_{e,t} P^{\text{d}}_{e,max} \tag{16}$$

$$E_{e,min} \le E_{e,t} \le E_{e,max}, \quad E_{e,T} = E_{e,1} \tag{17}$$

$$E_{e,t} = E_{e,t-1} + \left(\eta^{\text{c}} P^{\text{c}}_{e,t} - P^{\text{d}}_{e,t}/\eta^{\text{d}}\right)\Delta t, \forall t \in \mathcal{T}\setminus\{1\} \tag{18}$$

where $P^{\text{c}}_{e,\max}, P^{\text{d}}_{e,\max}, E_{e,\max}, E_{e,\min}, \eta^{\text{c}}$ and η^{d} represent maximum charging, discharging power, storage capacity, minimum energy level, charging and discharging efficiency, respectively. Δt is the time resolution. $E_{e,1}$ and $E_{e,T}$ are the energy levels at the beginning and end of a day.

2.2.4. Controllable Thermal Loads

With the popularity of inverter-based heaters and air conditioners, the cooling and heating systems in smart buildings have become flexible resources [24]. Considering the acceptable range of human thermal comfort, the power consumption process of the controllable thermal loads is modeled in an adjustable specific limit. It can provide both upward and downward flexibility within the temperature settings. The operational region of thermal load is formulated as follows.

$$H_{b,t} = H_{b,t-1} - (H_{b,t-1} - H^{\text{env}}_{b,t-1})/(RC) - \eta P^{\text{e2h}}_{b,t-1}/C \tag{19}$$

$$H_{b,\min} \le H_{b,t} \le H_{b,\max} \tag{20}$$

$$P^{\text{e2h}}_{b,\min} \le P^{\text{e2h}}_{b,t} \le P^{\text{e2h}}_{b,\max} \tag{21}$$

Equation (19) represents the thermal dynamics of buildings. R and C are the thermal resistance and capacitance of the building envelope. $H^{\text{env}}_{b,t}$ is the ambient temperature around building b at time t. η is the power to heat coefficient as positive for cooling and negative for heating. Constraint (20) represents the acceptable temperature range within $[H_{b,\min}, H_{b,\max}]$. Constraint (21) denotes the available power consumption range within $[P^{\text{e2h}}_{b,\min}, P^{\text{e2h}}_{b,\max}]$.

2.3. Power Exchange Model

In this work, the DS and VPPs are co-optimized to reduce power loss. DS and MVPPs exchange power at the point of common coupling (PCC). Therefore, a coupling constraint (22) guarantees that the scheduled power at the DS side equals that at the VPP side.

$$P^{\text{tds}}_{k,t} = P^{\text{fvpp}}_{k,t} \tag{22}$$

2.4. Peak Ramp Minimization Model

Power systems usually deal with intense ramping issues in transmission and distribution systems collaboratively. However, the flexibility in the transmission network may not be sufficient to support the ramping demand with the high penetration of renewable energy. As an intermediary entity between the

transmission and distribution networks, the DSO is responsible for ramping management [22]. It restrains the highest power ramps at the distribution transformer level to provide ancillary service for the upstream transmission system [25]. In this context, the coordinated peak ramp minimization model is formulated as

$$\textbf{(OP)}: \min_{\boldsymbol{x},\boldsymbol{P}} \ f \quad \text{s.t. (4)-(22).} \tag{23}$$

3. Decentralized Solution Approach

The problem (**OP**) can be solved using a centralized approach, which requires large computational resources and access to complete information from multiple entities. To address these issues, we design a novel decentralized framework that preserves local information, leveraging the Lagrangian relaxation and KKT conditions.

Constraints (4) and (22) serve as global inequality and equality constraints coupling the DS and VPPs. In the proposed decentralized approach, we formulate an augmented Lagrangian function for (OP) by relaxing constraints (4) and (22) as follows.

$$\begin{aligned} L = f + \sum_{t\in\mathcal{T}} \omega_t^{\mathrm{l}}(-r_t-\phi) + \sum_{t\in\mathcal{T}} \omega_t^{\mathrm{u}}(r_t-\phi) + \sum_{t\in\mathcal{T}}\sum_{k\in\mathcal{K}} \omega_{k,t}(P_{k,t}^{\mathrm{fvpp}} - P_{k,t}^{\mathrm{tds}}) \\ + \frac{\rho}{2}\sum_{t\in\mathcal{T}}\sum_{k\in\mathcal{K}} \|P_{k,t}^{\mathrm{fvpp}} - P_{k,t}^{\mathrm{tds}}\|_2^2 \end{aligned} \tag{24}$$

It is observed that L is unbounded, as the ϕ-related terms can be positive or negative infinity. Let $\omega_t^{\mathrm{l}*}$ and $\omega_t^{\mathrm{u}*}$ be the optimal multiplier. According to stationarity condition $\frac{\partial L}{\partial \phi} = 0$, equality equation $\sum_{t\in\mathcal{T}}(\omega_t^{\mathrm{u}*} + \omega_t^{\mathrm{l}*}) = a_1$ holds. Then, the ϕ-related term is eliminated by adding KKT stationarity condition to the problem. As a result, the new Lagrangian function exclusively comprises locally separable variables for individual DS or VPP. Based on the Lagrangian relaxation and KKT condition, the primal problem can be decomposed into a DSO sub-problem (SP-DSO) and K VPP sub-problems (SP-VPPk), which will be shown soon.

By separating the decision variables for DSO, we formulate the objective function for DSO

$$\begin{aligned} L^{\mathrm{d}}\left(\boldsymbol{P}^{\mathrm{dso}}, \boldsymbol{\omega}\right) = a_2 \sum_{t\in\mathcal{T}}\Big(c_{0,t}P_{1,t} + \sum_{i\in\mathcal{I}} P_{i,t}\Big) + \sum_{t\in\mathcal{T}}\sum_{k\in\mathcal{K}} \omega_{k,t}P_{k,t}^{\mathrm{fvpp}} \\ + \frac{\rho}{2}\sum_{t\in\mathcal{T}}\sum_{k\in\mathcal{K}} \|P_{k,t}^{\mathrm{fvpp}} - \hat{P}_{k,t}^{\mathrm{tds}}\|_2^2, \end{aligned} \tag{25}$$

where the decision variables $\boldsymbol{P}^{\mathrm{dso}}$ of the DSO are denoted as $\boldsymbol{P}^{\mathrm{dso}} = [P_{i,t}, P_{k,t}^{\mathrm{fvpp}}, Q_{i,t}]$.

Then, the DSO subproblem can be formulated as follows. It receives $\hat{P}_{k,t}^{\mathrm{tds}}$ from VPP k in the last iteration. Then, it broadcasts $P_{k,t}^{\mathrm{fvpp}}$ to the VPPs after local optimization.

$$\textbf{(SP-DSO)}: \max_{\boldsymbol{\omega}} \min_{\boldsymbol{P}^{\mathrm{dso}}} L^{\mathrm{d}}\left(\boldsymbol{P}^{\mathrm{dso}}, \boldsymbol{\omega}\right) \quad \text{s.t. (5)-(10)}$$

Similarly, by separating the decision variables for VPP k, we get the objective function as

$$\begin{aligned} L_k^{\mathrm{v}}\left(\boldsymbol{P}_k^{\mathrm{vpp}}, \boldsymbol{\omega}\right) = f_k^{\mathrm{vpp}} - \sum_{t\in\mathcal{T}}\left(\omega_{k,t} - \omega_t^{\mathrm{l}} + \omega_t^{\mathrm{u}} + \omega_{t+1}^{\mathrm{l}} - \omega_{t+1}^{\mathrm{u}}\right)P_{k,t}^{\mathrm{tds}} \\ + \frac{\rho}{2}\sum_{t\in\mathcal{T}} \|\hat{P}_{k,t}^{\mathrm{fvpp}} - P_{k,t}^{\mathrm{tds}}\|_2^2, \end{aligned} \tag{26}$$

where the decision variables $\boldsymbol{P}_k^{\mathrm{vpp}}$ of the VPP are denoted as $\boldsymbol{P}_k^{\mathrm{vpp}} = [P_{m,t}^{\mathrm{pv}}, P_{k,t}^{\mathrm{tds}}, P_{g,t}^{\mathrm{mgt}}, P_{e,t}^{\mathrm{es}}, P_{b,t}^{\mathrm{e2h}}]$.

Then, the subproblem for VPP k can be formulated as follows. It receives $\hat{P}_{k,t}^{\mathrm{fvpp}}$ from DSO in the last iteration. Then, it broadcasts $P_{k,t}^{\mathrm{tds}}$ to the DSO after local optimization.

$$\textbf{(SP-VPPk)}: \max_{\boldsymbol{\omega}} \min_{\boldsymbol{P}_k^{\mathrm{vpp}}} L_k^{\mathrm{v}}\left(\boldsymbol{P}_k^{\mathrm{vpp}}, \boldsymbol{\omega}\right) \quad \text{s.t. (11)-(21)}$$

The DSO and VPP subproblems can be solved independently. Specifically, the DSO's optimization problem is tackled given the exported power from VPPs and updated dual variables. Each VPP optimizes its own problem using information about the imported power from the DS and corresponding multipliers. The Lagrange multipliers of constraints (22) are updated by

$$\omega_{k,t}^{Cnt+1} = \omega_{k,t}^{Cnt} + \alpha\{P_{k,t}^{\mathrm{fvpp}} - P_{k,t}^{\mathrm{tds}}\}. \tag{27}$$

Based on the KKT condition, we define the feasible set of multipliers associated with constraints (4) as $\Gamma \triangleq \left\{\{\omega_t^{\mathrm{u}}, \omega_t^{\mathrm{l}}\} | \sum_{t\in\mathcal{T}}(\omega_t^{\mathrm{u}} + \omega_t^{\mathrm{l}}) = a_1, \omega_t^{\mathrm{u}}, \omega_t^{\mathrm{l}} \geq 0\right\}$.

The Lagrange multipliers for constraints (4) are updated in the feasible region following

$$\omega_t^{\mathrm{l},Cnt+1} = \Pi_\Gamma\left\{\omega_t^{\mathrm{l},Cnt} + \alpha(-r_t)\right\} \triangleq \Pi_\Gamma\left\{\tilde{\omega}_t^{\mathrm{l},Cnt}\right\}, \tag{28}$$

$$\omega_t^{\mathrm{u},Cnt+1} = \Pi_\Gamma\left\{\omega_t^{\mathrm{u},Cnt} + \alpha(r_t)\right\} \triangleq \Pi_\Gamma\left\{\tilde{\omega}_t^{\mathrm{u},Cnt}\right\}, \tag{29}$$

where α is the step size. The second term of equations (28) and (29) are the unbiased estimate of the subgradient of the Lagrangian function. $\Pi_\Gamma(\boldsymbol{\lambda}) = \arg\min_{\omega}\{\|\boldsymbol{\lambda} - \boldsymbol{\omega}\| | \boldsymbol{\omega} \in \Gamma\}$ is the Euclidean projection of $\boldsymbol{\lambda}$ onto feasible set Γ, which can be formulated as the following optimization problem.

$$\textbf{(EP)}: \min \ \frac{1}{2}\|\boldsymbol{\lambda} - \boldsymbol{\omega}\|_2^2 \ \text{s.t.} \sum_{t\in\mathcal{T}}(\omega_t^{\mathrm{u}} + \omega_t^{\mathrm{l}}) = a_1, \omega_t^{\mathrm{u}}, \omega_t^{\mathrm{l}} \geq 0 \tag{30}$$

We can derive the projection by solving the problem (**EP**) based on the KKT condition as

$$\omega_t^{\mathrm{A},Cnt+1} = \begin{cases} \tilde{\omega}_t^{\mathrm{A},Cnt} - \gamma^*, & if\ \gamma^* \leq \tilde{\omega}_t^{A,Cnt} \\ 0, & otherwise \end{cases} \tag{31}$$

where the superscript $\mathrm{A} \in \{\mathrm{l}, \mathrm{u}\}$ is used to distinguish multipliers ω_t^{u} and ω_t^{l}. γ^* is a unique solution of equation $\sum_{t\in\mathcal{T}}\left\{\max\{\tilde{\omega}_t^{\mathrm{u}} - \gamma, 0\} + \max\{\tilde{\omega}_t^{\mathrm{l}} - \gamma, 0\}\right\} = a_1$.

Finally, the proposed ADMM-like algorithm is summarized in Algorithm1.

Algorithm 1: ADMM-like Decentralized Optimization

Input: Load:$L^{\mathrm{p}}_{i,t}$, $L^{\mathrm{q}}_{i,t}$;Electricity price:$c_{0,t}$;Weights: a_i.
Init.: Iteration $Cnt \leftarrow 0$, tolerance Δ, multipliers ω.
Formulate the SP-DSO and SP-VPPk based on Lagrangian relaxation and KKT condition.
while $Cnt \leq N_{Cnt}$ or $Gap \geq \Delta$ **do**
  Receive the $\hat{P}^{\mathrm{tds}}_{k,t}$ from VPP k. Solve the DSO subproblem **SP-DSO**.
  Broadcast optimized exchange $P^{\mathrm{fvpp}}_{k,t}$ to the VPPs;
  Receive the $\hat{P}^{\mathrm{fvpp}}_{k,t}$ from DSO. Solve the VPP subproblems **SP-VPPk**.
  Broadcast optimized exchange $P^{\mathrm{tds}}_{k,t}$ to the DSO;
  Calculate primal objective Z^{p}, dual objective Z^{d}, and the optimality gap $Gap = Z^{\mathrm{p}} - Z^{\mathrm{d}}$;
  Update Lagrange multipliers according to (27), and (29).
  Update $Cnt \leftarrow Cnt + 1$;
Output: Exchanged power with main grid $P_{1,t}$ & VPP $P^{\mathrm{tds}}_{k,t}$.

4. Case Study

In this section, simulations are conducted to validate the efficiency and effectiveness of the proposed model and distributed algorithm. First, it is demonstrated using the IEEE 69-node distribution system. Subsequently, the scalability of the approach is analyzed through simulations on the IEEE 141-node distribution system. The proposed models are implemented in MATLAB R2020b and solved using MOSEK 10.2. All simulations are carried out on a PC with Intel(R) Core(TM) i5-9500 CPU @ 3.00GHz and 32 GB of RAM.

4.1. IEEE 69-node System

The one-line diagram of the IEEE 69-node distribution system is depicted in Fig. 2. Three VPPs are connected to nodes -25, -44, and -63 in the distribution system, respectively. Consistent with previous studies [7, 8], VPPs aggregate DERs at the same node and engage in power exchange via PCC. A total of 30 PV, 30 MGT, 200 CTL, and 3 BES are distributed among the VPPs. The hourly demand is based on a normalized load profile derived from PJM, a regional transmission organization in the United States, for April 3, 2024. It is scaled by 3.8 MW to the DS load level. Additionally, LMP data for the same date is sourced from PJM within the RTO [26]. Solar power profile data is sampled from open-source data of Austria in 2016 [27]. Each MGT's capacity is randomly generated between 30-60 kW, while BES has a capacity of 100 kW*2h. The temperature of CTL is limited to 22-26°C. The reference temperature is set to 24°C. The ambient temperature data is sourced from *Time and Date AS* of Washington, DC, USA, on July 13, 2023 [28]. Unit costs for MGT and PV are set at \$25/MWh and \$10/MWh respectively. Objective weights are specified as $a_1 = 0.4, a_2 = 0.3$, and $a_3 = 0.3$.

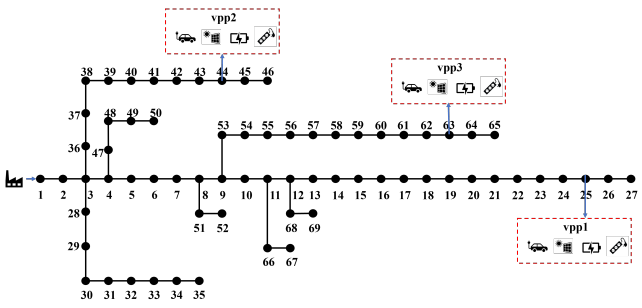

Figure 2: The 69-node distribution system with 3 VPPs.

4.1.1. Effectiveness of Peak Ramp Minimization Model

Case studies are conducted to validate the effectiveness of the proposed peak ramp minimization model. Detailed dispatch results in three VPPs are presented in Fig. 3. The CTL consumes more power and storage charges during valley periods. In addition, the MGT provides more power and storage discharges during peak periods Fig. 4 shows the optimized output of MVPPs and the exchanged power between the PDN and the main grid. The results show that MVPPs predominantly supply the load during peak periods, effectively smoothing the load peaks. Notably, original peak ramping events at 6:00 and 9:00 give an upward ramping demand of 0.505 MW/h and a downward ramping demand of 0.422 MW/h. In contrast, the optimized scenario depicts maximum ramping events occurring at 4:00 and 16:00, albeit with a reduced downward ramping demand of 0.153 MW/h and an upward ramping demand of 0.158 MW/h. It shows that the proposed model yields a reduction of 68.7% and 63.7% in the upward and downward peak ramping, respectively. It also reveals the model's potential to reduce the peak-valley difference, mitigating it from 1.558 MW to 1.333 MW.

Table 2: The comparison of model performance.

Model	upward peak ramp	downward peak ramp	power losses
Case 1	0.158 MW/h	0.153 MW/h	2.988 MWh
Case 2	1.180 MW/h	0.639 MW/h	3.057 MWh
Case 3	0.222 MW/h	0.255 MW/h	3.261 MWh

The impact of modeling ramping regulation and power loss can be analyzed via

- Case 1: Proposed model;
- Case 2: Do not consider ramping regulation;
- Case 3: Do not consider power loss minimization.

According to Table 2, *Case 2* has an upward peak ramp of 1.180 MW/h, and downward peak ramps of 0.639 MW/h, which are higher than that of *Case 1*. The difference reflects *Case 2*'s prioritization of economic performance while overlooking the ramping burden. The results demonstrate a substantial reduction of 86.61% in upward ramping demand and 76.06% in downward ramping demand in our proposed model. That effectively eases the ramping burden for the main grid. Power losses constitute approximately 3.82%, 4.06%, and 4.17% of the total power supplied in three cases. The slight distinction in power

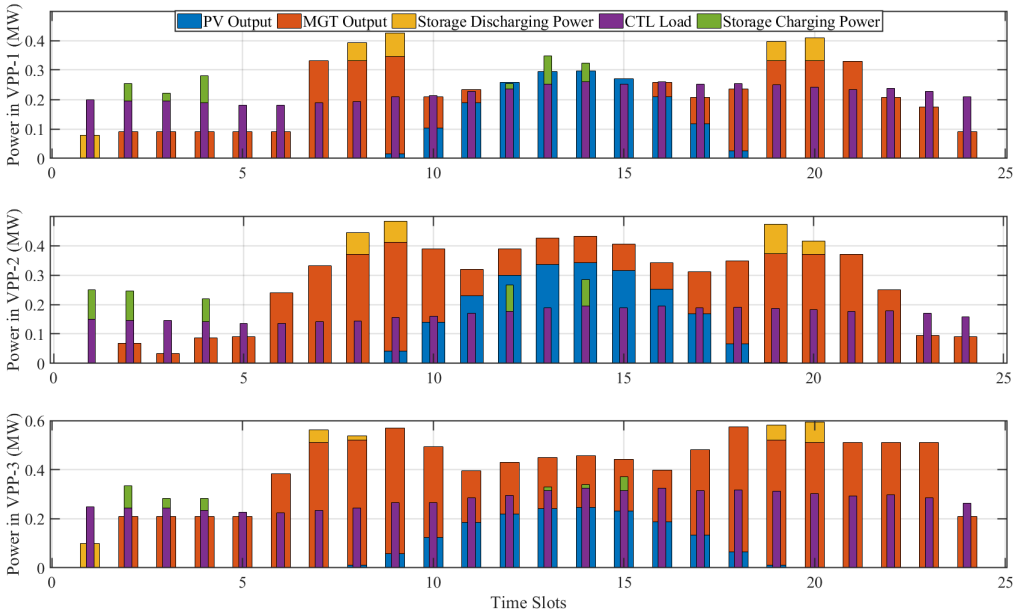

Figure 3: The power combination of different DERs in each VPP.

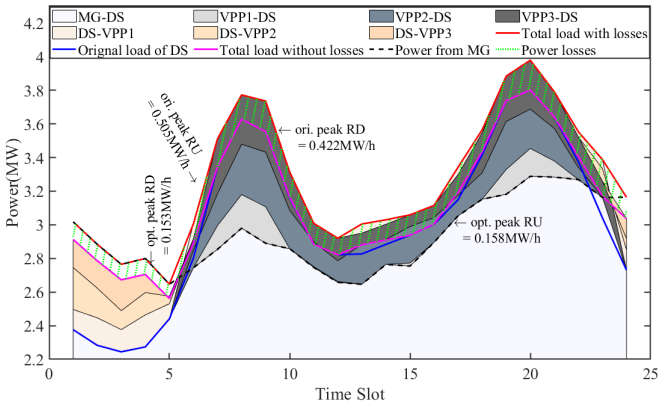

Figure 4: The demand is served by main grid and MVPPs.

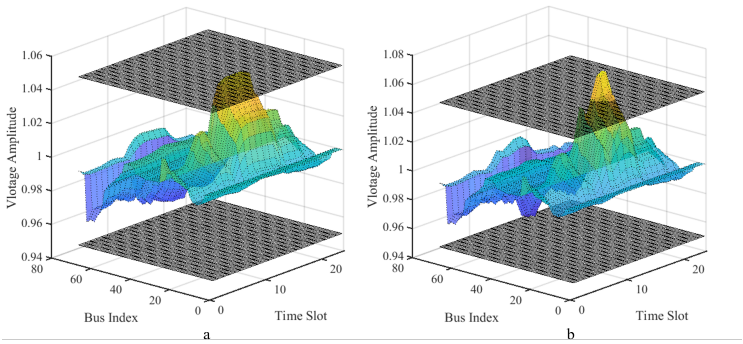

Figure 5: (a) The voltage profile obtained by the location-aware model. (b) The voltage profile obtained by the model in [21].

losses is attributed to different power flow patterns with different objectives. In *Case 3*, the power loss is 6.67% and 9.14% higher than *Case 1* and *Case 2*, respectively. Therefore, not accounting for power losses would underestimate the economic performance of the DSO. It indicates that the proposed model can mitigate the ramping burden and power losses.

4.1.2. Location-aware VPP's Impact on Power Loss and Voltage

To investigate the impact of location-aware VPP coordination on power losses and voltage, the PV, MGT, and load are set to be 5, 3, and 1.2 times in this subsection for the future scenario. For comparison, the method proposed in [21] without considering the location-aware information is selected as a benchmark to validate the effectiveness of our formulation. The corresponding power losses and voltage information are listed in Table 3. It is observed that the power losses obtained by our formulation are 5.7% (i.e. 2.749-2.592)/2.749) lower than the non-location-aware model. Fig.5(a) and Fig.5(b) show the voltage profiles optimized from our model and the comparison model, respectively. It is observed that overvoltage occurs in the non-location-aware model. For instance, the maximum voltage is 1.065 p.u. on bus-25 at 15:00. In addition, there are 1.21% voltage violations without considering location-aware VPP connection information. In contrast, the voltages obtained with our model are all within the secure limit. This suggests that overlooking VPP locations, as is common in most literature, may result in voltage violations.

4.1.3. Convergence of ADMM-like Algorithm

To demonstrate the convergence of the proposed distributed algorithm, Fig. 6 (a) depicts the primal and dual objective val-

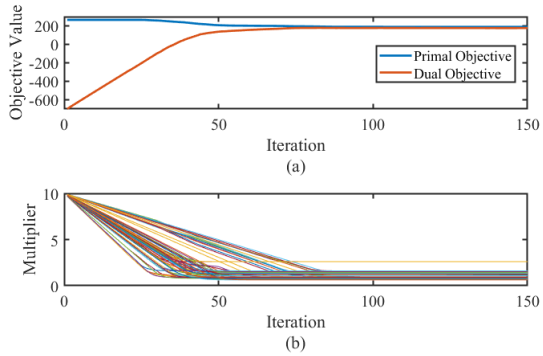

Figure 6: (a) The primal and dual objectives converge with iterations.(b) The multipliers converge with iterations.

Table 3: The effectiveness of the location-aware model.

Model	power losses	maximum voltage	voltage violation ratio
Our formulation	2.592 MWh	1.050 p.u.	0
Model in [21]	2.749 MWh	1.065 p.u.	1.21%

ues over iterations. It is observed that the primal objective steadily decreases with iterations, while the dual objective generally exhibits an increasing trend. Notably, the proposed distributed algorithm converges after approximately 81 iterations. The optimality gap approaches almost 0 following convergence. The average computational time per iteration is about 1.859 seconds with a parallel structure. Fig. 6 (b) illustrates the convergence trend of multipliers in (27) versus iteration. Furthermore, it should be noted that the sum of multipliers in (29) equals a_1, satisfying the KKT condition.

4.1.4. Impact of Flexibility from Thermal Load

To explore the impact of thermal loads on ramping management, the sensitivity analysis is conducted by changing the thermal comfort deviation penalty factor a_3 from 0.01 to 1. The detailed hourly temperature and electrical power consumption of controllable thermal loads are depicted in Fig. 7. As shown in Fig.7 (a), the temperature increases sharply during 4:00-7:00 and 16:00-18:00 in most scenarios. Correspondingly, the power consumption of controllable thermal loads shown in Fig.7 (b) is lower during 4:00-7:00, which is optimized to ease the upward ramping burden. However, the power consumption during 16:00-18:00 is high due to the high ambient temperature. Similarly, the temperature has a decreasing trend during 7:00-9:00 and 18:00-21:00. In the first temperature-dropping period, the CTL begins pre-cooling to increase power consumption and reduce the downward ramping burden. The temperature decreases during 18:00-21:00 as the ambient temperature drops. In Fig.7 (b), the controllable thermal load curve presents a valley during the evening peak at 19:00. This is because a wider tolerance of temperature deviation can be acceptable as the penalty factor decreases, reducing power consumption. The results indicate that the CTL partly alleviates the ramping burden.

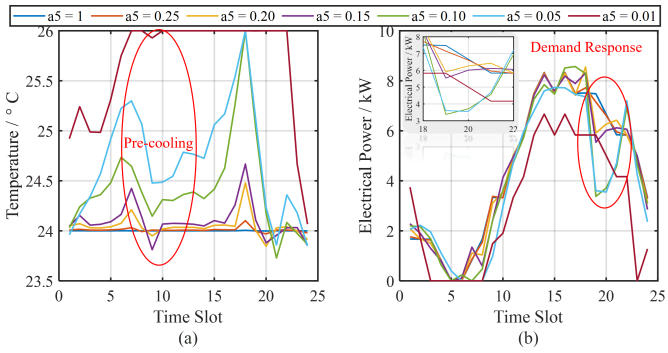

Figure 7: (a) Temperature and (b) electrical power of controllable thermal load with different weighted factors.

4.1.5. Privacy Preservation and Computation Burden

Upon exploring the structure of the subproblems, it is observed that only the Lagrangian multiplier and the quantity of exchanged power are needed to achieve the optimal solution. This observation highlights the effectiveness of the proposed distributed algorithm in preserving the privacy of DSO and VPP entities.

The computational complexity of different model scales can be analyzed via

- Case 1: 30 PVs, 30 MGTs, 3 ESs, and 120 CTL;
- Case 2: 60 PVs, 60 MGTs, 3 ESs, and 240 CTL.

Table 4 presents a comparative analysis of the model scale between the proposed ADMM-like and the centralized MIP methods. In the ADMM-like method, the largest sub-model is the DSO subproblem. According to the first two rows, the proposed method reduces the number of variables by 11.00% and the number of constraints by 17.53%. Comparing the cases with different numbers of DERs, it is found that the MIP's scale experiences a rapid increase with the increment of DERs. In contrast, the ADMM-like model scale remains unaffected, as the largest subproblem is the SP-DSO with a limited number of DERs.

Furthermore, the subproblems can be solved locally within each VPP agent in parallel. This mechanism can reduce the computational burden and improve efficiency. Notably, the MIP's runtime exhibits a steeper increase than the ADMM-like method in a larger model. For example, when the number of DER doubles, the running time of MIP and ADMM-like methods in each iteration increases by 175% (i.e. 6.396-2.327)/2.327, and 24% (i.e. 2.306-1.859)/1.859, respectively. It indicates that the proposed method substantially alleviates computational burden, particularly in scenarios with large-scale DERs or VPPs.

Table 4: The comparison of computational complexity between centralized MIP and decentralized ADMM-like model.

Case	Model	# var.	# cons.	Non-zeros	Time (s)[a]
Case 1	MIP	22,273	28,200	90,354	2.327
	ADMM-like	19,824	23,256	82,272	1.859
Case 2	MIP	34,657	58,440	138,450	6.396
	ADMM-like	19,824	23,256	82,272	2.306

[a] Averaged running time of each iteration.

4.1.6. Accuracy vs. Efficiency Estimation

To estimate the balance between solution accuracy and computational efficiency of the proposed model, a *Trade-off Ratio* is defined using the ratio of solution accuracy (e.g., relative optimality gap compared to a benchmark MIP solution) to computational time (e.g., Running time per iteration * Iterations).

$$\textit{Trade-off Ratio} = \frac{\textit{Optimality Gap/Benchmark MIP Objective}}{\textit{Computational Time}}$$

By setting different convergence conditions (e.g., relative optimality gap), the computational time is recorded and plotted in Fig. 8. We mark the red pentagram as a knee point. The points to the right of the red pentagram show only small gains in accuracy, while incurring a significant increase in computational cost. In contrast, the points to the left side of the red pentagram have good accuracy improvement, with only a slight increase in computational cost. Therefore, the marked red pentagram can be regarded as a trade-off between the solution accuracy and the computational efficiency, offering better accuracy for a similar computational cost.

4.1.7. Impact of the Energy Storage Lifecycle

To explore the impact of the energy storage's lifecycle on peak ramp minimization, the lifecycle limits are added into the model following the cycle counting method in [29] and the operation cycles limit in [30]. In this part, the daily storage cycles are set to less than 2. The detailed operation status of different storage without and with lifecycle limit is presented in

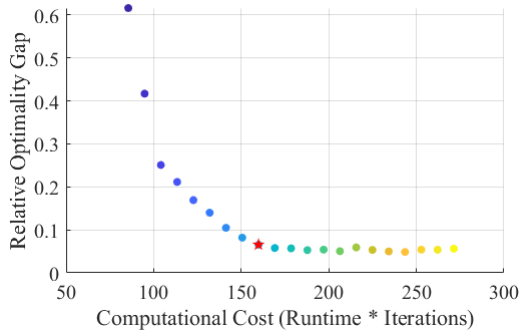

Figure 8: The trade-off ratio between solution accuracy and computational efficiency.

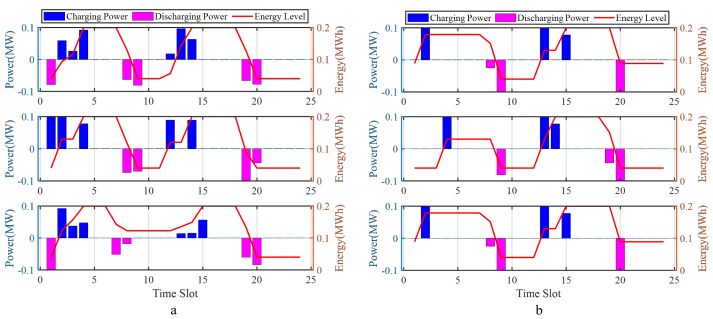

Figure 9: Schedule of BES with and without operation cycles limit.

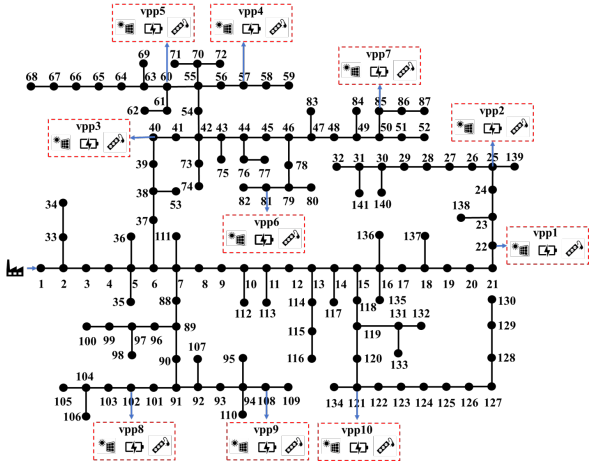

Figure 10: The 141-node distribution system with 10 VPPs.

Fig. 9(a) and Fig. 9(b). It is observed that the cycles of three storage without cycle limit are 2, 2, and 1.5 while all of them are 1.5 with the limit. Due to the operation cycle limit, the optimized upward and downward are 0.324 MW/h and 0.426 MW/h, which are 104% and 176% higher than case 1. It indicates that the operation cycle limit restricts the flexibility of the storage system.

4.2. IEEE 141-node System

To evaluate the scalability of the proposed solution method, we further conduct simulations on the IEEE 141-node distribution power system with 10 VPPs, as depicted in Fig. 10. Within these VPPs, a total of 500 PVs, 500 MGTs, 120 CTLs, and 10 BESs are distributed. The capacity of each BES is set to be 400 kW*2h. Other parameter settings remain consistent with those used in the IEEE 69-node system cases.

4.2.1. Scalability of ADMM-like Algorithm

In the IEEE 141-node system, the total number of buses, VPPs, and DERs increased by 2.04, 3.33, and 31.9 times, respectively, compared to the 69-node system. In contrast, the computational time of the proposed ADMM-like algorithm implemented on the 141-node system increases only 2.33 times per iteration compared to the 69-node system. The DER dispatches in each VPP is shown in Fig. 11. The peak loads are mainly served by the MVPPs, reducing the continuous upward ramping demands. The CTL partly fills the load valley at night. The aggregated dispatch results of MVPPs and DS are summarized in Fig. 12. In the proposed model, it is reduced to 0.751 MW/h at 15:00 compared to the original ramping of 1.174 MW/h at 6:00. To balance ramping cost and energy cost, a new valley is formed, although it does not increase the downward ramping demands. The downward peak ramp is reduced from 1.258 MW/h at 9:00 to 0.625 MW/h at 23:00. Besides, the peak-valley difference decreases from 5.445 MW to 3.670 MW. This indicates that the proposed ADMM-like algorithm scales efficiently to larger systems.

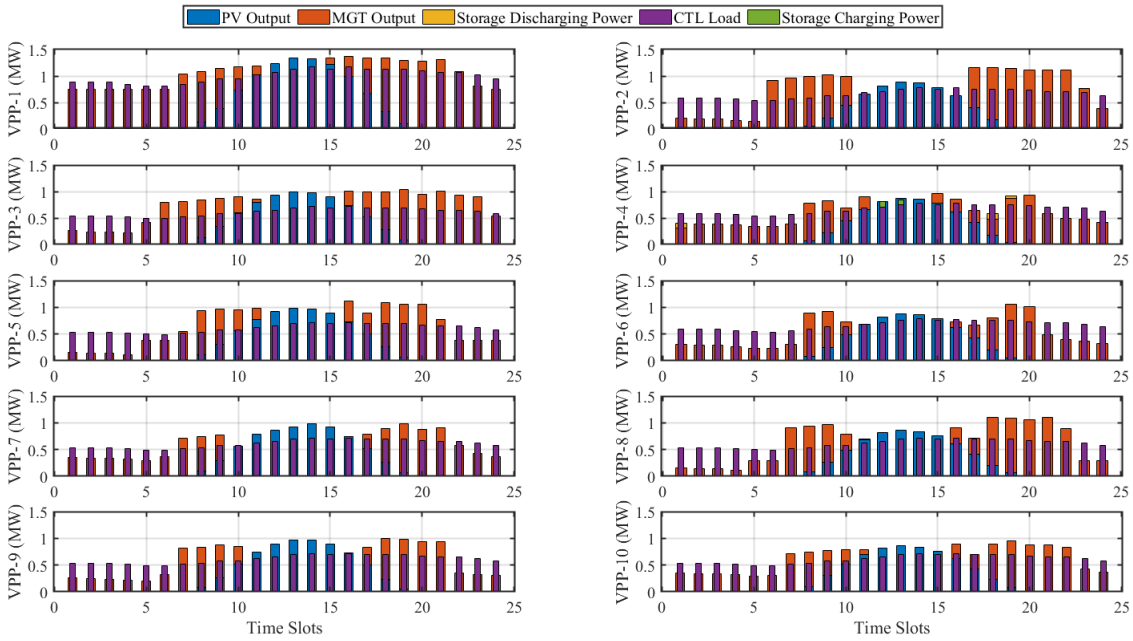

Figure 11: DER dispatches in each VPP.

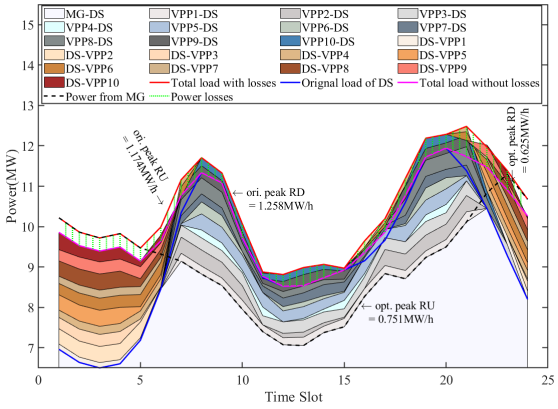

Figure 12: The power exchange among PDN, main grid, and MVPPs.

4.2.2. *Comparison With Conventional ADMM*

In this part, we compare the proposed algorithm with the classic ADMM method, summarizing the results in Table 5. For solution quality assessment, we compare the objectives of centralized MIP, decentralized ADMM, and decentralized ADMM-like methods. The objectives of different methods vary within a deviation to the optimum of 2.01%. Regarding computational efficiency, we compare the model scale, solving time per iteration, iteration times, and memory occupation. Compared to centralized MIP, the ADMM and ADMM-like methods have a much smaller model for each distributed DSO or VPP agent, leading to approximately 63.7% memory savings compared to MIP when solving the optimization problem. As a side note, the ADMM model is slightly larger than the ADMM-like model due to the additional variables and constraints associated with the maximum ramping. Additionally, the average calculation

Table 5: ADMM-like Alg. Performance on IEEE 141-node Sys.

Model	# Var.	# Cons.	Time	# Iteration	Peak Memory	Obj.	Info. Exchange
MIP	71,929	112,152	19.415 s	-	16.510 GB	976.31	60,200
ADMM	40,729	47,832	4.471 s	89	5.536 GB	981.80	10,464
ADMM-like	40,728	47,784	4.325 s	101	5.525 GB	995.95	312

time of the decentralized methods is about 4.5 times faster than MIP. It is worth noting that the calculation time of ADMM and ADMM-like methods is almost the same due to the similar model scale. Nevertheless, the non-relaxed constraints (4) in ADMM contribute to faster convergence, resulting in fewer iterations. Regarding privacy preservation, we analyze the information exchange process. The centralized MIP requires full information on VPPs and DS, whereas the proposed ADMM-like method only needs information on power exchange and dual multipliers between VPPs and DSO. ADMM requires additional information as it has to broadcast the DS hourly load information to VPPs. All the nodes have to send their local load information to the DSO and then the DSO broadcasts it to all VPPs in the ADMM mechanism. Its communication cost is higher. Considering it, ADMM will have a larger communication overhead to transmit information among multiple agents than the ADMM-like method. The last column of the table shows that the ADMM-like method requires the exchange of only 312 parameters, which is greatly fewer than the MIP (60,200 parameters) and ADMM (10,464 parameters) methods. This indicates that the proposed ADMM-like method has an advantage over ADMM in terms of privacy preservation and communication. As analyzed above, the proposed ADMM-like algorithm demonstrates a computationally efficient solution to the large-scale distributed VPP aggregation problem preserving privacy.

5. Conclusion

This paper introduces a novel peak ramp minimization model for modern power distribution systems featuring multi-VPPs. The proposed model incorporates location-aware power exchanges to reduce distribution losses and operational costs while mitigating ramping burdens. To address computational and communication challenges, a decentralized ADMM-like algorithm is introduced based on KKT conditions, enabling local optimization and preserving the private information of individual VPPs. Simulation results validate the effectiveness of the proposed framework in terms of efficiency, accuracy, and privacy preservation. The coordinated operation between the distribution system operator and MVPPs demonstrates significant reductions in power losses, operational costs, and peak ramp events. In our future research, we plan to address uncertainties related to prices, demand, and renewable energy sources.

References

[1] U.S. EIA, International energy outlook, Report, U.S. Energy Information Administration (EIA) (2023).

[2] IEA , Unlocking the potential of distributed energy resources, Report, IEA, Paris https://www.iea.org/reports/unlocking-the-potential-of-distributed-energy-resources (2022).

[3] S. Fattaheian-Dehkordi, A. Rajaei, A. Abbaspour, M. Fotuhi-Firuzabad, M. Lehtonen, Distributed transactive framework for congestion management of multiple-microgrid distribution systems, IEEE Trans. Smart Grid 13 (2) (2022) 1335–1346. doi:10.1109/TSG.2021.3135139.

[4] T.-C. Ou, H. Tieng, T.-H. Tsai, Y.-Y. Li, M.-H. Hung, F.-T. Cheng, Design of green power clouds for intelligent virtual power plants, IEEE Trans. Autom. Sci. Eng. (2024) 1–12doi:10.1109/TASE.2024.3406412.

[5] M. Vahedipour-Dahraie, H. Rashidizadeh-Kermani, M. Shafie-Khah, J. P. S. Catalão, Risk-averse optimal energy and reserve scheduling for virtual power plants incorporating demand response programs, IEEE Trans. Smart Grid 12 (2) (2021) 1405–1415. doi:10.1109/TSG.2020.3026971.

[6] G. Mohy-ud din, K. M. Muttaqi, D. Sutanto, Adaptive and predictive energy management strategy for real-time optimal power dispatch from vpps integrated with renewable energy and energy storage, IEEE Trans. Ind. Appl. 57 (3) (2021) 1958–1972. doi:10.1109/TIA.2021.3057356.

[7] Z. Yi, Y. Xu, J. Zhou, W. Wu, H. Sun, Bi-level programming for optimal operation of an active distribution network with multiple virtual power plants, IEEE Trans. Sustain. Energy 11 (4) (2020) 2855–2869. doi:10.1109/TSTE.2020.2980317.

[8] M. Zhang, Y. Xu, H. Sun, Optimal coordinated operation for a distribution network with virtual power plants considering load shaping, IEEE Trans. Sustain. Energy 14 (1) (2023) 550–562. doi:10.1109/TSTE.2022.3220276.

[9] S. Boyd, N. Parikh, E. Chu, B. Peleato, J. Eckstein, Distributed optimization and statistical learning via the alternating direction method of multipliers, Found. Trends Optim. (2011). doi:10.1561/2200000016.

[10] N. F. Avila, C.-C. Chu, Distributed probabilistic atc assessment by optimality conditions decomposition and lhs considering intermittent wind power generation, IEEE Trans. Sustain. Energy 10 (1) (2019) 375–385. doi:10.1109/TSTE.2018.2796102.

[11] Y. Ge, H. Ye, K. A. Loparo, Agent-based privacy preserving transactive control for managing peak power consumption, IEEE Trans. Smart Grid 11 (6) (2020) 4883–4890. doi:10.1109/TSG.2020.2997314.

[12] Z. Li, M. Shahidehpour, Privacy-preserving collaborative operation of networked microgrids with the local utility grid based on enhanced benders decomposition, IEEE Trans. Smart Grid 11 (3) (2020) 2638–2651. doi:10.1109/TSG.2019.2959242.

[13] S. Shao, F. Gao, J. Wu, Distributed multi-area intraday economic dispatch using modified critical region projection algorithm, IEEE Trans. Autom. Sci. Eng. 21 (2) (2024) 2074–2087. doi:10.1109/TASE.2023.3252659.

[14] C. Feng, K. Zheng, Y. Zhou, P. Palensky, Q. Chen, Update scheduling for admm-based energy sharing in virtual power plants considering massive prosumer access, IEEE Trans. Smart Grid 14 (5) (2023) 3961–3975. doi:10.1109/TSG.2023.3243811.

[15] L.-N. Liu, G.-H. Yang, Distributed optimal energy management for integrated energy systems, IEEE Trans. Ind. Informat. 18 (10) (2022) 6569–6580. doi:10.1109/TII.2022.3146165.

[16] Z. Tang, D. J. Hill, T. Liu, Fast distributed reactive power control for voltage regulation in distribution networks, IEEE Trans. Power Syst. 34 (1) (2019) 802–805. doi:10.1109/TPWRD.2018.2868158.

[17] L.-N. Liu, G.-H. Yang, Distributed fixed-time optimal resource management for microgrids, IEEE Trans. Autom. Sci. Eng. 20 (1) (2023) 404–412. doi:10.1109/TASE.2022.3155163.

[18] H. Gao, J. Liu, L. Wang, Z. Wei, Decentralized energy management for networked microgrids in future distribution systems, IEEE Trans. Power Syst. 33 (4) (2018) 3599–3610. doi:10.1109/TPWRS.2017.2773070.

[19] S. Patel, M. Ahmed, S. Kamalasadan, A novel energy storage-based net-load smoothing and shifting architecture for high amount of photovoltaics integrated power distribution system, IEEE Trans. Ind. Appl. 56 (3) (2020) 3090–3099. doi:10.1109/TIA.2020.2970380.

[20] H. Ebrahimi, A. Yazdaninejadi, S. Golshannavaz, Decentralized prioritization of demand response programs in multi-area power grids based on the security considerations, ISA Transactions 134 (2023) 396–408. doi:https://doi.org/10.1016/j.isatra.2022.07.031.

[21] H. K. Nguyen, A. Khodaei, Z. Han, Incentive mechanism design for integrated microgrids in peak ramp minimization problem, IEEE Trans. Smart Grid 9 (6) (2018) 5774–5785. doi:10.1109/TSG.2017.2696903.

[22] S. Fattaheian-Dehkordi, A. Abbaspour, M. Fotuhi-Firuzabad, M. Lehtonen, A distributed framework for intense ramping management in distribution networks, IEEE Trans. Smart Grid 14 (1) (2023) 315–327. doi:10.1109/TSG.2022.3199811.

[23] Z. Yang, H. Zhong, A. Bose, T. Zheng, Q. Xia, C. Kang, A linearized opf model with reactive power and voltage magnitude: A pathway to improve the mw-only dc opf, IEEE Trans. Power Syst. 33 (2) (2018) 1734–1745.

[24] X. Sun, H. Xie, Y. Xiao, Z. Bie, Incentive compatible pricing for enhancing the controllability of price-based demand response, IEEE Trans. Smart Grid 15 (1) (2024) 418–430. doi:10.1109/TSG.2023.3279415.

[25] S. I. Gkavanoudis, K.-N. D. Malamaki, E. O. Kontis, C. S. Demoulias, A. Shekhar, U. Mushtaq, S. B. Venu, Provision of ramp-rate limitation as ancillary service from distribution to transmission system: Definitions and methodologies for control and sizing of central battery energy storage system, Journal of Modern Power Systems and Clean Energy 11 (5) (2023) 1507–1518. doi:10.35833/MPCE.2022.000595.

[26] PJM. [2024]. data package [data miner 2], `https://dataminer2.pjm.com/list`, accessed 3/15,2024.

[27] Open power system data. [2016]. data package [renewables.ninja pv and wind profiles]. version [2020-09-16]. [www.renewables.ninja], `https://data.open-power-system-data.org/`, accessed 7/10,2022.

[28] Time and Date. [2024]. data package [weather], `https://www.timeanddate.com/`, accessed 6/5,2024.

[29] R. Nebuloni, L. Meraldi, L. Moretti, V. Ilea, C. Bovo, A. Berizzi, P. Raboni, A real-time cycle counting method for battery degradation calculation in milp models, in: 2023 IEEE International Conference on Environment and Electrical Engineering and 2023 IEEE Industrial and Commercial Power Systems Europe (EEEIC / I&CPS Europe), 2023, pp. 1–6. doi:10.1109/EEEIC/ICPSEurope57605.2023.10194776.

[30] H. Ebrahimi, A. Yazdaninejadi, S. Golshannavaz, Demand response programs in power systems with energy storage system-coordinated wind energy sources: A security-constrained problem, Journal of Cleaner Production 335 (2022) 130342. doi:https://doi.org/10.1016/j.jclepro.2021.130342.